Four Current Examples of Characterization of Silicon Carbide

S. Bai[1], Yue Ke[1], Y. Shishkin[1], O. Shigiltchoff[1], R.P. Devaty[1], W.J. Choyke[1]
D. Strauch[2], B. Stojetz[2], B. Dorner[3], D. Hobgood[4], J. Serrano[5], M. Cardona[5], H. Nagasawa[6], T. Kimoto[7], and L.M. Porter[8]
[1]Dept. of Physics and Astronomy, Univ. of Pittsburgh, Pittsburgh 15260, PA, USA
[2]Institut für Theoretische Physik, Universität Regensburg, 93040 Regensburg, Germany
[3]Institut Laue-Langevin, 38042 Grenoble, France
[4]Cree, Inc., 4600 Silicon Drive, Durham, NC 27703
[5]Max-Planck-Institut, Heisenbergstrasse 1, 70569 Stuttgart, Germany
[6]Hoya Advanced Semiconductor Technologies Co. Ltd., Kanagawa 229-1125, Japan
[7]Dept. of Electronic Science & Engineering, Kyoto University, Kyoto 606-01, Japan
[8]Dept. of Mat. Sci., Carnegie Mellon Univ., Pittsburgh, PA 15213, USA

ABSTRACT

A description is given of the profiling of CVD grown 3C SiC on undulant (001) Si using low temperature photoluminescence (LTPL). Inelastic neutron scattering (INS) and X-ray Raman scattering (XRS) are compared for acoustical modes of 4H SiC. Schottky barrier heights are obtained for 4H and 6H SiC on different crystal faces using three different measuring techniques. Scanning electron microscopy (SEM) is used to display a variety of porous SiC morphologies achieved in n-type and p-type SiC.

This paper is intended to be the introduction to the “CHARACTERIZATION” section of this volume. To serve this purpose we illustrate the subject matter with new results using four distinct experimental techniques.

A. LOW TEMPERATURE PHOTOLUMINESCENCE (LTPL) PROFILING OF THICK EPITAXIAL 3C SIC GROWN ON UNDULANT (001) SI

Introduction

The first wave of 3C SiC epitaxial growth on (001) Si was started in 1983 [1]. These efforts produced thin films of less than 20µm, with a high density of lattice defects. When removed from the Si substrates they were extremely fragile and subject to cleaving into small strips. These phenomena were studied in numerous papers [2-5]. Growth of improved quality 3C-SiC films on 6H SiC substrates was demonstrated in 1989 [6]. For the next decade homoepitaxy of 4H and 6H SiC reigned supreme. Nagasawa and colleagues renewed the interest in 3C SiC with their introduction of 3C SiC grown on “undulant” (001) Si large diameter substrates [7]. Here we shall report on the LTPL profiling of a 219µm thick 3C SiC layer grown on undulant (001) Si.

Experimental procedure

LTPL measurements were performed on a large, 219µm thick 3C SiC film cut into a number of pieces. We irradiated the samples with a 30mW He-Cd laser (325nm) at 2K and measured the 3C SiC film front surface whilst on the (001) Si substrate. We then removed the film from the

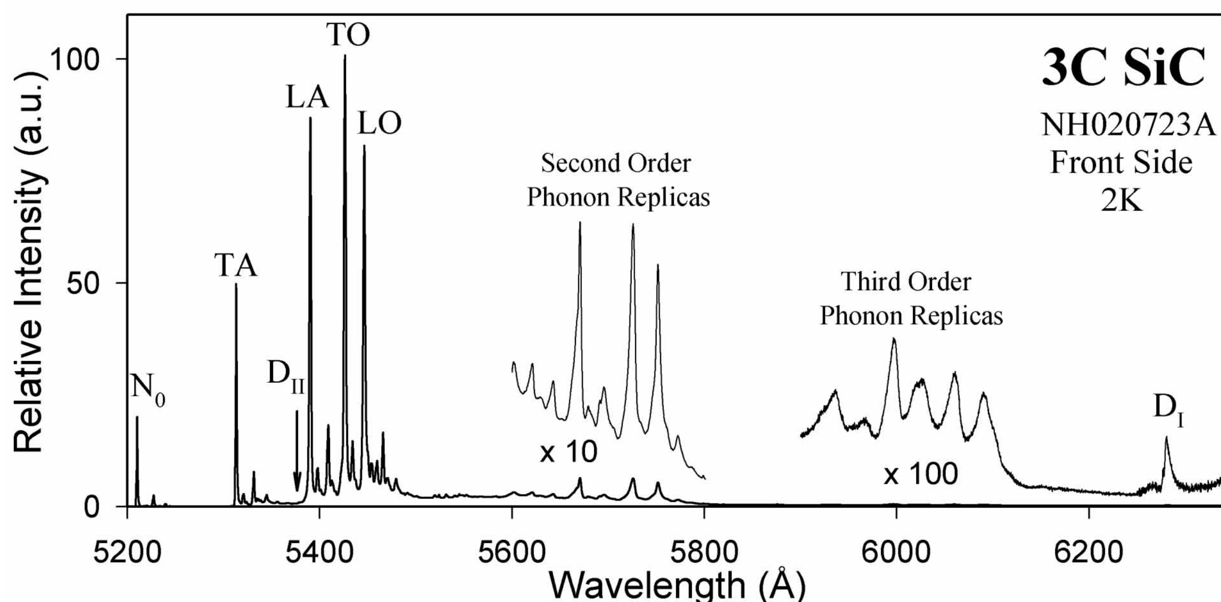

Figure 1. 2K spectrum of the "front" side of a 219 μm thick 3C SiC film removed from undulant (001) Si. The "back" side is the side which was separated from the undulant (001) Si substrate. N_0 is the no-phonon line of the exciton bound to the neutral nitrogen donor and TA, LA, TO, and LO are first order phonon replicas. D_{II} and D_I are the two most common intrinsic defects seen in SiC by means of optical experiments.

substrate and measured the front and back surfaces of the free standing film. Subsequently we thinned the free standing 3C SiC film to 205μm, 150μm and 110μm and again measured the front and back surfaces.

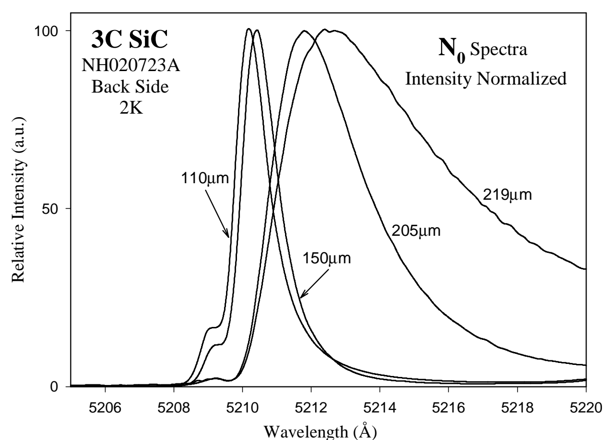

Figure 2. The N_0 line as measured from the "back" of the sample. The sample was successively thinned to 205 μm, 150 μm, and 110μm.

Results and discussion

In figure 1 we have a global picture of the 2K, 3C SiC LTPL spectrum measured from the front of the 219μm thick film after removal from the (001) Si substrate. The most notable features are marked as follows: N_0 is the nitrogen no-phonon line at 5210Å, D_{II} is an intrinsic defect whose no-phonon line is at 5373Å, TA-LA-TO-LO are the first order phonon replicas of N_0, the ranges of the second and third order phonon replicas of N_0 are marked, and lastly we indicate D_I, at 6279Å, the most common intrinsic defect in SiC observed by means of optical experiments.

On figure 2 we show a normalized and expanded view of the N_0 lines measured from the "back" of the samples for all the thicknesses

of our 3C SiC film. We are not certain as to the nature of the small high energy satellite on the high energy side of N_0. The largest stress shift towards lower energies is seen for the 219μm film. It is about 1meV which is smaller than the 4meV to 7meV shifts towards lower energy observed from the front of thin (10μm) SiC films of 3C SiC grown on ordinary (001) Si [3].

Figure 3 shows the diminution of the D_{II} defect no phonon line measured from the "back" with thinning of the film. The D_{II} defect was reported 30 years ago [8], but its very nature is still the subject of active theoretical investigation. It is certainly a carbon related complex but the final verdict is not yet in. Normally, this defect is observed in heavily implanted samples subsequent to high temperature annealing. It has been reported once before in 3C SiC grown on undulant (001) Si [9].

Figure 4 shows the normalized D_I defect spectrum measured on the "back" side as a function of film thickness. D_I is the most common intrinsic defect in SiC observed by means of optical experiments. It was first described in 3C SiC in 1971 [10]. It is seen that the line marked L of the 219μm film is shifted slightly (1meV) towards lower energy and is much broader than the line at 110μm. This shift is quite similar to the measured red shift of the N_0 no-phonon line. For the 110μm film, the L line of the D_I center has a high energy satellite (an excited state) marked M using the notation of [10]. Since 1971 there has been a spate of papers which have attempted to pinpoint the nature of this defect center in SiC. The model that is currently most accepted is the "pseudo donor" model [11]. Recent theoretical calculations attribute the D_I defect center to the neutral anti-site pair [12].

Summary and conclusion

We have measured the LTPL spectra of a film of 3C SiC grown heteroepitaxially on undulant (001) Si as a function of the removal of 3C SiC material from the side of the film which

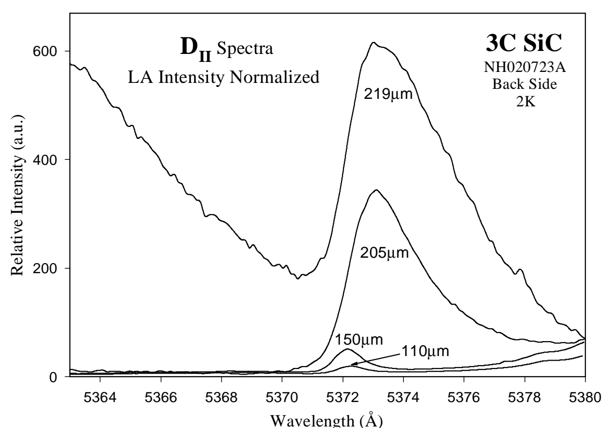

Figure 3. The D_{II} no-phonon line, where the LA phonon replica is normalized such as to show the relative strength of the D_{II} line as material is removed from the "back" of the sample.

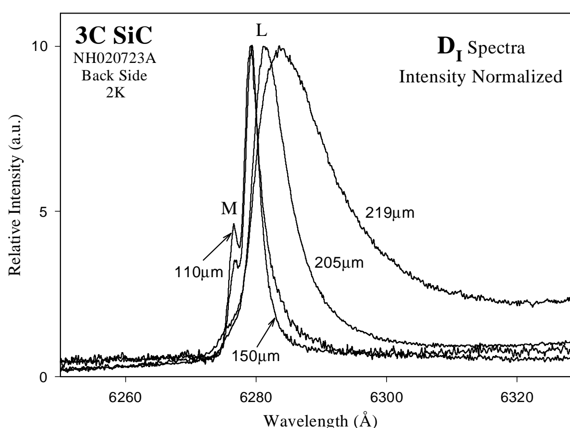

Figure 4. The D_I no-phonon line, measured from the "back" of the sample with intensities being normalized. As the sample is thinned to 150μm the D_I line becomes sharp enough to reveal an excited state M of the L line.

originally faced the (001) Si substrate. There is a maximum stress shift of 1meV to lower energy for the N_0 line as well as the L line of the D_I center and a somewhat smaller shift (0.4meV) for the no-phonon line of the D_{II} center. The diminution of the defect centers D_I and D_{II} as we remove material from the interface between the 3C SiC and the (001) Si is quite consistent with the microstructural findings in 3C SiC [7] grown in this fashion.

B. A COMPARISON OF X-RAY RAMAN SCATTERING AND INELASTIC NEUTRON SCATTERING IN DETERMINING PHONON DISPERSION CURVES OF 4H SIC

Introduction

Interest in the lattice dynamics of the polytypes of SiC goes back forty years. In the sixties single crystal samples of SiC were far too small to attempt neutron scattering, even though high flux research reactors were being put into operation at that time and were being successfully used to measure the lattice branches in Diamond and Silicon. Our primary information about the lattice phonons of SiC polytypes came from low temperature photoluminescence [13-16], infrared reflectivity [17,18] and Raman scattering [19]. Finally, in the late nineties the first phonon dispersion curves were obtained in 6H SiC by inelastic neutron scattering (INS) [20] using a three axis neutron spectrometer situated at the hot source of the Institut Laue-Langevin (ILL) in Grenoble. X-ray Raman scattering was brought to bear recently on 3C SiC [21] and 4H SiC [22] using the European Synchrotron Radiation Facility (ESRF) beam line ID28 also in Grenoble. After first reviewing the X-ray Raman data for 3C SiC and 4H SiC, we report on preliminary results of an extensive study of the acoustical branches of 4H SiC obtained by INS at ILL. Due to the fact that the "hot burner" at ILL was still being refurbished (May 2002) the measurements of the optical modes were postponed until more energetic neutrons are available in 2003.

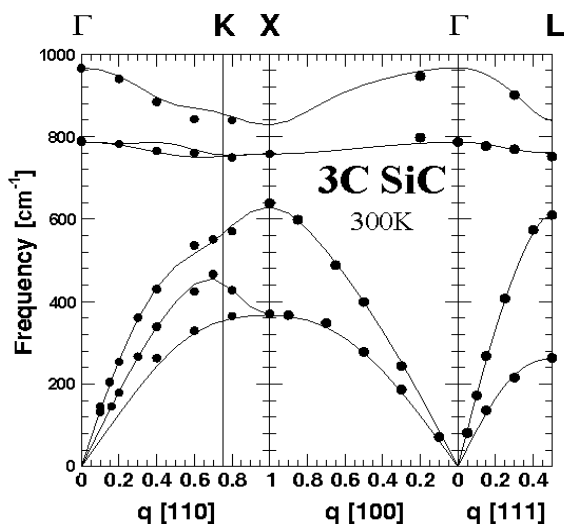

Figure 5. Phonon dispersion relations of 3C SiC. XRS data is shown by filled circles and the solid lines are calculated dispersion curves.

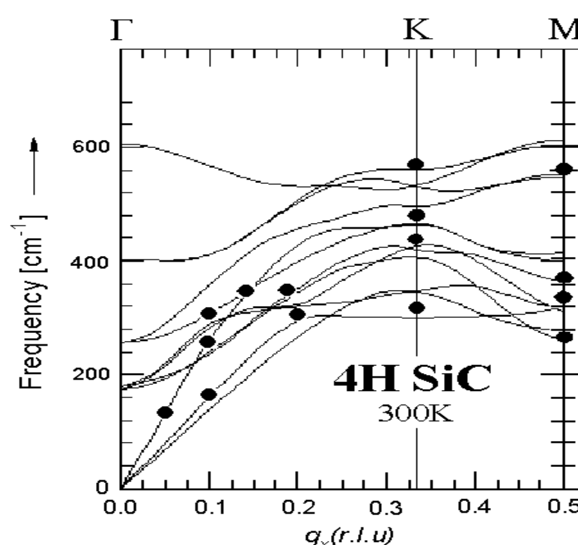

Figure 6. Acoustic phonon dispersion curves of 4H SiC. Full circles are XRS data and solid lines are calculated phonon dispersion curves. The $\vec{q}$-axis is given in reciprocal lattice units (r.l.u).

Experiment

High quality crystals of 3C SiC are still only available in small size, far too small for INS. However, the high brilliance third generation synchrotron radiation available at ESRF makes possible studies of the phonon dispersion of 3C SiC by means of X-ray Raman scattering (XRS)/ Inelastic X-Ray Scattering (IXS) with crystals a few millimeters in size. Two such n-type crystals with less than $10^{16}cm^{-3}$ nitrogen were selected after extensive LTPL and Laue transmission measurements. TA(X), LA(X), TO(X) and LO(X) were determined for the two samples to be $372.6cm^{-1}$ /$372.6cm^{-1}$, $641cm^{-1}$/$639.6cm^{-1}$, $765.4cm^{-1}$/$763.0cm^{-1}$, $834.0cm^{-1}$/ $830.0cm^{-1}$ respectively. The phonon dispersion curves obtained with X-ray Raman scattering are given in figure 5. The figure is taken from the paper by J. Serrano et al. [21]. The phonons determined by LTPL and XRS at the X point on the Brillouin zone boundary are in excellent agreement. Similar XRS experiments were carried out with specimens obtained from a large clear 4H SiC single crystal with $N_D - N_A = 2 \times 10^{17}cm^{-3}$. The crystal was cut to make samples with (0001), $(1\bar{1}00)$ and $(11\bar{2}0)$ faces. After polishing down with 1/4 µm diamond paste the samples were given a chemical polish with a final 4Å RMS surface roughness. Sample sizes were $8x8mm^2$, $8x13mm^2$ and $8x9mm^2$ and were 0.58mm in thickness. The acoustical phonon dispersion relations obtained by XRS on these samples [22] are given in figure 6. Agreement with the data obtained by LTPL is excellent [23,24]. Obtaining a sample of high enough quality and size for detailed INS examination is a tribute to the great effort expended in developing the high temperature boule growth of single crystal polytypes of SiC. The sample used in the INS/ILL studies whose preliminary results we shall now report on has dimensions of $18.5x24x24mm^3$. It is n-type 4H SiC with a nitrogen concentration deduced from 2K LTPL to be $2x10^{15}cm^{-3}$. It was carefully oriented with (0001), $(1\bar{1}00)$ and $(11\bar{2}0)$ faces and polished to a good optical finish. The

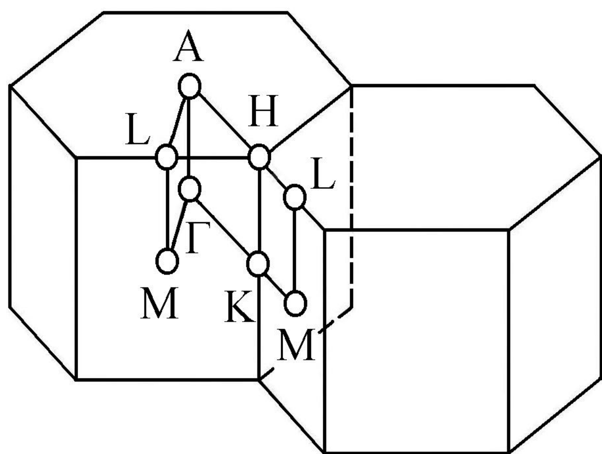

Figure 7. Brillouin zone for hexagonal polytypes.

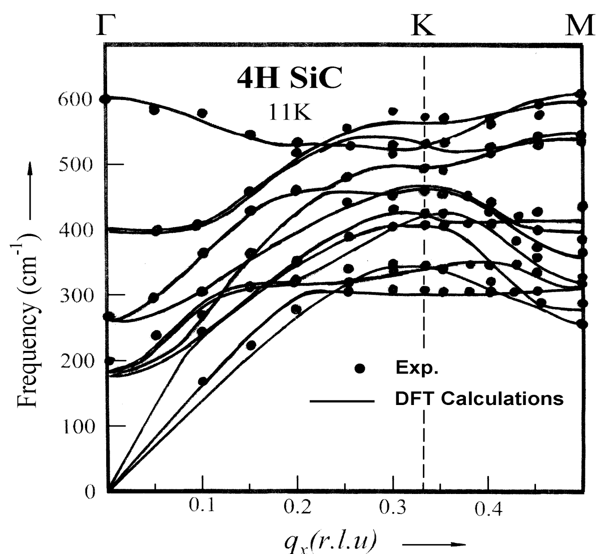

Figure 8. Acoustic phonon dispersion curves of 4H SiC measured by INS. Full circles are INS data points and solid lines are calculated phonon dispersion curves.

Brillouin zone for hexagonal polytypes is shown in figure 7. We performed experiments on the Γ--K--M, K--H, M--L, A--H--L and Γ--M--L lines for frequencies up to about 650cm^{-1}. Here we shall only discuss the Γ--K--M line. The results are shown on figure 8. These experiments were carried out at 11K as compared to 300K for the XRS of the 4H SiC. It was possible to obtain a higher density of data points than for the XRS data, but only acoustical data was obtained thus far. Data for the other directions will be reported in a future detailed paper. In figure 8 the data are compared to semi-empirical calculations. The (harmonic) ABC force constants are calculated using ab initio density functional perturbation theory for 3C SiC (stacking sequence ABCABC..., where every letter depicts one SiC layer). The ABA force constants are calculated for 2H SiC (stacking sequence ABAB...). These force constants have been used for 4H SiC (stacking sequence BABCBABC...).

Conclusion

It has been shown that XRS is now feasible for small crystal samples of SiC using high brightness synchrotron radiation. Using large single crystals of SiC polytypes detailed phonon dispersion curves may now also be obtained by means of INS using high flux nuclear research reactors.

C. SCHOTTKY BARRIER HEIGHTS FOR 4H AND 6H SIC: COMPARISON OF I-V, C-V AND INTERNAL PHOTOEMISSION MEASUREMENTS

Introduction

We have undertaken an investigation of the dependence of the Schottky barrier height on the crystal faces of 4H and 6H SiC. Specifically, we are studying the $(0001)_{Si}$, $(000\bar{1})_{C}$, $(1\bar{1}00)$ and $(1\bar{2}10)$ faces using Ti, Mo and Pt as the metals. We have reported preliminary results [25,26]. Here we present a comparison of the three methods that we use to measure the Schottky barrier height: Current-Voltage (I-V), Capacitance-Voltage (C-V) and Internal Photoemission (IPE). Relatively few contacts provide acceptable data for more than one of the methods. The data that we discuss here are selected from hundreds of contacts. We analyze the data for all three techniques using conventional methods [27]. Going back over twenty years, many authors have discussed the role of spatial inhomogeneity of the Schottky barrier height on the behavior of the contacts. Refs. [28-32] are representative examples. Here, we assume a Gaussian distribution of barrier heights and fit the corresponding model expressions to our I-V and IPE data. Application of this model leads to improvement in the agreement of values of the Schottky barrier height determined by two or, in a few cases, all three techniques. When the values disagree, the value determined by C-V is usually the larger. The preparation of the 4H and 6H SiC boule pieces, CVD epitaxial growth, fabrication of ohmic and Schottky contacts and the experiments are discussed elsewhere [25,26]. The diameters of the Schottky contacts are 0.12 mm, 0.5 mm and 1.0 mm. However, no results for 0.12 mm diameter contacts appear on figures 9-12. All IPE measurements are performed on 1.0 mm diameter contacts.

Determination of the Schottky barrier height

In addition to conventional analyses [27], we attempt to account for spatial inhomogeneity at

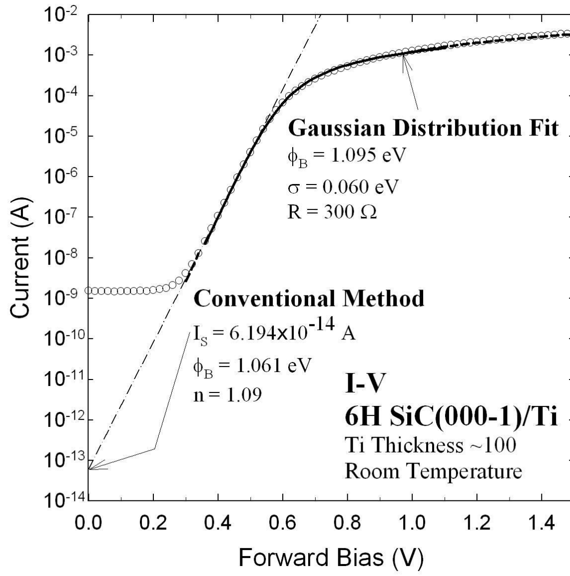

Figure 9. I-V data (circles) for a 6H SiC(000$\bar{1}$) /Ti contact, diameter 0.5 mm. The dash-dotted line shows the extrapolation of the linear region to determine the saturation current I_S, which is used to determine φ_B by the conventional method. The slope determines the ideality factor n. The thick solid line, extrapolated as dashes to cover data points not used in the fitting, shows the fit using the Gaussian distribution model.

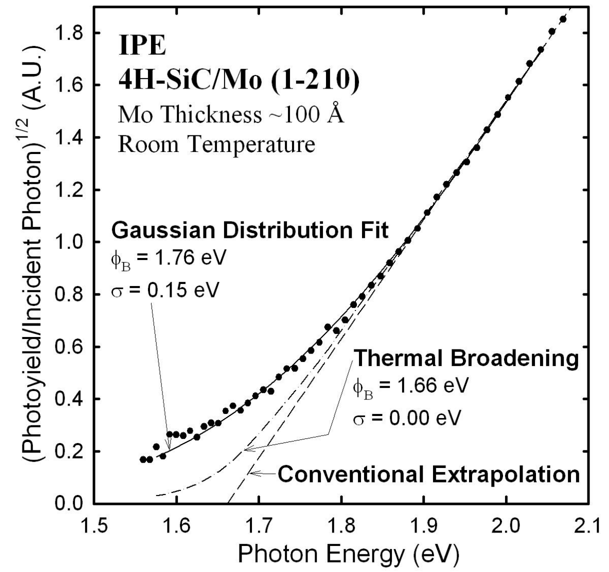

Figure 10. Internal Photoemission data (circles) for a 4H SiC(1$\bar{2}$10)/Mo contact, diameter 1 mm. The dashed line shows the extrapolation of the linear region to its energy axis intercept, conventionally interpreted as φ_B. The dash-dotted curve shows the effect of thermal broadening near the onset of IPE. The solid line shows the fit using the Gaussian distribution model.

the SiC-metal interface by introducing a Gaussian distribution of barrier heights:

$$\rho(\phi) = \frac{1}{\sqrt{2\pi}\sigma}\exp\left[-\frac{(\phi-\phi_B)^2}{2\sigma^2}\right],$$

where $\rho(\varphi)\,d\varphi$ is the probability that the barrier height is between φ and $\varphi + d\varphi$, φ_B is the mean Schottky barrier height and σ determines the width of the distribution.

To analyze I-V data, we assume that each member of the distribution behaves according to thermionic emission, in parallel with the rest of the members. In this model it is essential to introduce series resistance R, not only to describe the behavior at larger forward voltages, but also to obtain the modification in slope described in the conventional method by the ideality factor n. The parameters φ_B, σ and R are adjusted to obtain a fit to the data, with φ_B taken as the Schottky barrier height for the contact. Figure 9 shows an example.

If the width of the depletion region exceeds the spatial scale of the inhomogeneities in the distribution of barrier heights, recent calculations [31] indicate that the conventional analysis of C-V measurements provides a good approximation to the mean φ_B.

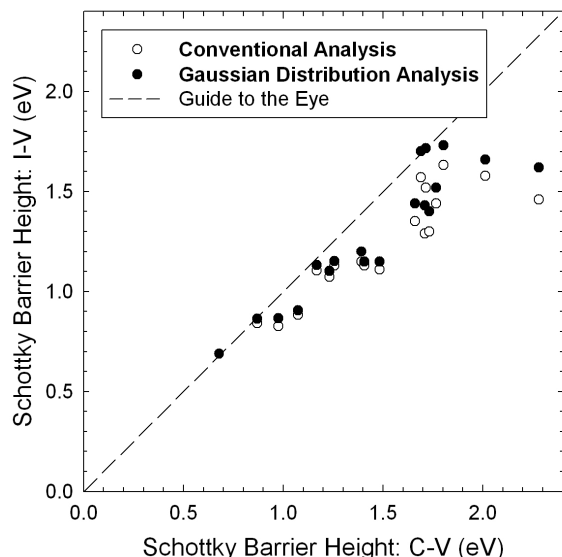

Figure 11. Comparison of Schottky barrier heights measured by I-V and C-V. Points on the dashed line correspond to agreement between the two methods. The open circles are results obtained using the conventional analysis of I-V data, whereas the solid circles were obtained by fitting the Gaussian distribution model to the data.

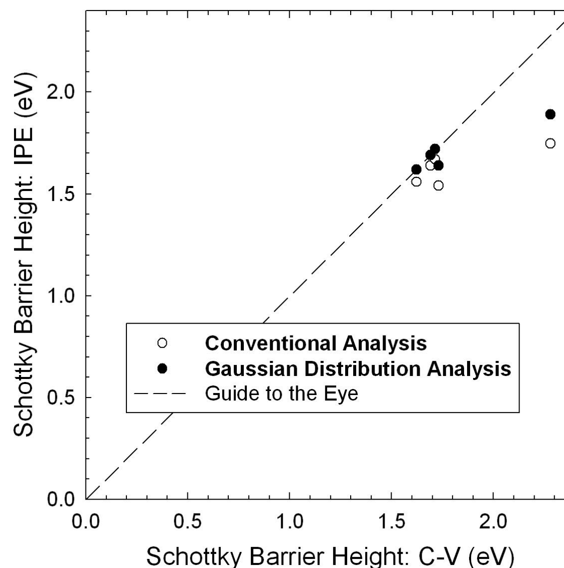

Figure 12. Comparison of Schottky barrier heights measured by IPE and C-V. Points on the dashed line correspond to agreement between the two methods. The open circles are obtained using the conventional analysis of IPE data, whereas the solid circles were determined by fitting the Gaussian distribution model to the data.

To interpret IPE data, the model includes the Gaussian distribution of barrier heights and the thermal broadening [33] described by the Fermi-Dirac distribution near the Fermi surface of the metal. We do not include the energy dependence of the density of electron states of the metal. The fitting parameters are φ_B, σ and an overall multiplicative constant C. Typical values of σ are comparable to or larger than values recently measured by BEEM (Ballistic Electron Emission Microscopy) on 6H SiC/Pd contacts [34]. Figure 10 shows a fit of this model to data, as an example. The resulting barrier height is larger by 0.10 eV than that obtained by the conventional analysis.

Discussion

The occurrence of contacts that provide acceptable data for at least two of the methods is relatively rare. The criteria for acceptable I-V data are: 1) at least 3-4 decades of linearity in the log(I) versus forward voltage plot and 2) an ideality factor n less than 1.4. C-V data were taken using three measurement frequencies: 10 kHz, 100 kHz and 1 MHz. For C-V data we require: 1) a region of linear behavior in $1/C^2$ versus reverse voltage extending at least from 0-2 V and preferably up to 10 V, 2) values of the doping concentration within a factor of two, obtained from data using the three frequencies, and 3) values of the band bending within 0.15 eV, obtained from data using the three frequencies (For all but four samples, the values of the band bending are within 0.05 eV. When there is a larger spread, the value obtained using 1 MHz

differs from the other two.). We have identified nineteen contacts that provide acceptable I-V and C-V data, and five that provide acceptable IPE and C-V data. Among these contacts are four that provide acceptable data for all three methods. There are no contacts that provide acceptable data for I-V and IPE alone. These relatively few contacts provide the basis for our comparison. The reason that such contacts are rare is that the experimental methods are not fully compatible. IPE measurements require large area contacts with thin metal layers of carefully controlled thickness. I-V and C-V measurements are best performed on low area contacts to avoid defects, but the precise thickness of the metal layer is not important. However, the contribution of edge effects increases with decreasing area.

Figure 11 presents a comparison of the Schottky barrier heights determined using I-V and C-V. Results using both the conventional method and the Gaussian distribution model are shown. The diagonal dashed line indicates the locus of points for which the two experimental methods agree. Note that there is a tendency for the C-V method to provide larger values for the Schottky barrier height. The analysis based on the Gaussian distribution leads to improved agreement.

Figure 12 is a plot of the Schottky barrier heights from IPE versus C-V. Although there are fewer points and they are rather bunched, the trends discussed in the preceding paragraph are also observed here. For the Gaussian distribution analysis, three of the five points lie essentially on the diagonal. Two of these points represent contacts for which agreement is obtained among all three techniques.

Conclusion

We have found that it is not easy to fabricate Schottky contacts for which acceptable data can be obtained using more than one of the three experimental methods available to us: Current-Voltage, Capacitance-Voltage and Internal Photoemission. For the relatively few contacts that provide results that can be compared, application of a fitting procedure based on the assumption of a Gaussian distribution of barrier heights leads to improved agreement between the values of the Schottky barrier height derived from the different experiments. When there is not agreement, the value obtained using C-V is generally the larger. It is clear that the fabrication of reproducible Schottky barriers on these four faces of 4H and 6H SiC using a variety of metals continues to be a challenge.

D. SCANNING ELECTRON MICROSCOPE (SEM) IMAGES OF VARIOUS MORPHOLOGIES OF N AND P-TYPE POROUS SIC

Introduction

The article in this volume by M. Mynbaeva presents much of the history, background chemistry and physics, as well as key references pertaining to porous SiC. Hence we will restrict ourselves here to discussing different morphologies which have recently been produced at the University of Pittsburgh, in both n and p-type SiC. We have attempted to characterize this porous SiC by ellipsometry, ultraviolet non-specular scattering and SEM. To date, only the SEM observations have proven to be a quick and successful way to judge the nature of the films that have been obtained.

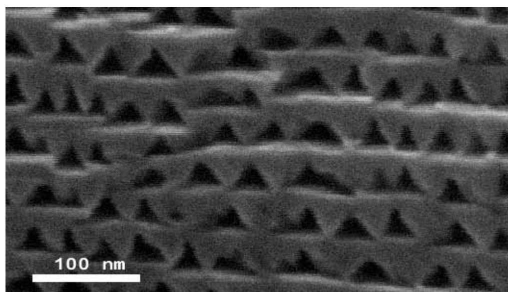

Figure 13. Triangular pore morphology of a 4H n-type SiC ($n = 6\times10^{18}$ cm^{-3}) sample etched at about 5 mA/cm^2 current density.

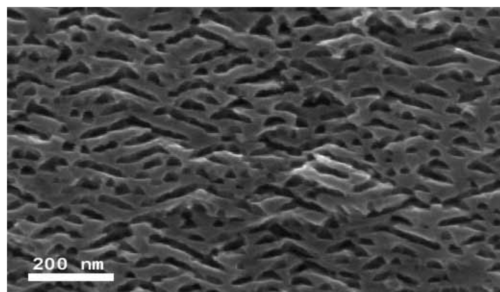

Figure 14. Chevron pore morphology of a 6H n-type SiC ($n = 3\times10^{18}$ cm^{-3}) sample etched at about 10 mA/cm^2 current density.

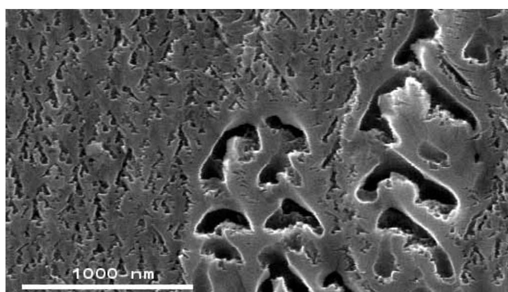

Figure 15. Tree-root with inclusions of seaweed pore morphology of a 6H n-type SiC ($n = 3\times10^{18}$ cm^{-3}) sample etched at about 30 mA/cm^2 current density.

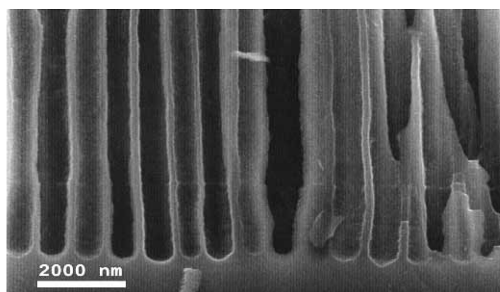

Figure 16. Asparagus pore morphology of a 4H n-type SiC ($n = 6\times10^{17}$ cm^{-3}) sample. Current density exceeds 100 mA/cm^2.

Experiment and discussion

Figures 13-16 present the results of photoelectrochemical etching on single crystal 4H and 6H n-type SiC with substrates doped with nitrogen from 6×10^{18} cm^{-3} down to 6×10^{17} cm^{-3}. The bath was 5% HF (by weight), 5% ethanol in distilled water. Current density values range from 5 mA/cm^2 to 75 mA/cm^2. Filtered UV radiation from a 300W Hg lamp is projected on to the interface between the crystal and the electrochemical bath. The intensity of this radiation is very roughly of the order of 10^{17} photons per cm^2. In contrast, figures 17-20 show the results of electrochemical etching in the dark of p-type 6H SiC ($p = 2.4\times10^{18}$ cm^{-3}) with current densities ranging from 1 mA/cm^2 to 30 mA/cm^2. For n-type substrates photon assistance is required to produce the triangular pore morphology and to a lesser extent the chevron pore morphology. Gradually we transform to the tree root morphology where photon assistance is a minor factor. There is a sharp threshold to a “seaweed” structure. This threshold region is seen on figure 15. Finally at high current density there emerges a structure which looks like asparagus. It should be noted that self supporting films of these structures have been prepared for thicknesses varying from seven to 70μm.

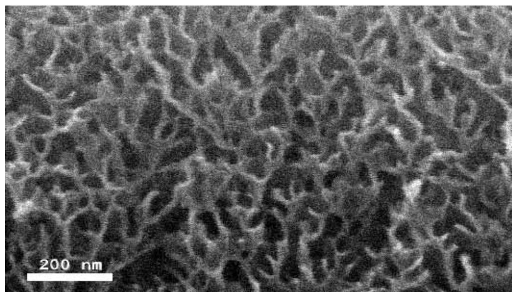

Figure 17. Algae morphology of a 6H p-type SiC ($p = 2.4\times10^{18}$ cm^{-3}) sample etched at 1 mA/cm^2. Pore walls ~ 15 – 30 nm.

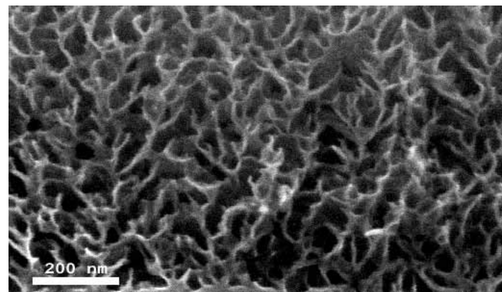

Figure 18. Algae morphology of a 6H p-type SiC ($p = 2.4\times10^{18}$ cm^{-3}) sample etched at 5 mA/cm^2. Pore walls ~ 10 – 25 nm.

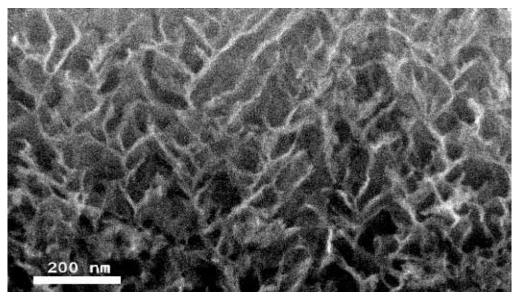

Figure 19. Algae morphology of a 6H p-type SiC ($p = 2.4\times10^{18}$ cm^{-3}) sample etched at 15 mA/cm^2. Pore walls ~ 5 – 15 nm.

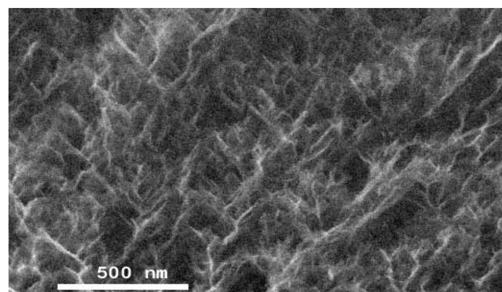

Figure 20. Cobweb morphology of a 6H p-type SiC ($p = 2.4\times10^{18}$ cm^{-3}) sample etched at 30 mA/cm^2. Pore walls ~ 1 – 10 nm.

Preparation of porous SiC in p-type material is quite different from that in n-type material. Thus far, we have mainly obtained an "algae" like morphology which gradually changes into something which resembles a "cobweb" as seen in the sequence shown on figures 17-20. The pore walls become progressively smaller with increased etching current density. We estimate that the thinnest walls in the 30 mA/cm^2 sample are in the 10 Å range. In this regime one might begin to observe quantum effects. Finally, it has been possible to prepare self supporting films of the porous p-type SiC.

Conclusion

A number of interesting applications have already been identified for porous SiC, in epitaxy, biological detectors and bone tissue engineering. In the future we expect porous SiC to present us with many exciting and unexpected uses.

ACKNOWLEDGEMENTS

We wish to thank ONR (grant N00014-01-1-0028), DURINT (grant N00014-01-1-0715) and NASA (grant NAG3-2538) for partial support for this work.

REFERENCES

1. S. Nishino, J. A. Powell and H.A. Will, Appl. Phys. Lett. **42**, 460 (1983).

2. P. Pirouz, C.M. Chorey and J.A. Powell, Appl. Phys. Lett. **50**, 221 (1987).
3. W.J. Choyke, Z.C. Feng and J.A. Powell, J. Appl. Phys. **64**, 3163 (1988).
4. Z.C. Feng, W.J. Choyke and J.A. Powell, J. Appl. Phys. **64**, 6837 (1988).
5. W.J. Choyke, J.A. Powell, T.T. Cheng and P. Pirouz, Mater. Sci. Forum **38-41**, 1433 (1989).
6. J.A. Powell, D.J. Larkin, L.G. Matus, W.J. Choyke, J.L. Bradshaw, L. Henderson, and M. Yoganathan, Appl. Phys. Lett. **56**, 1353 (1990).
7. H. Nagasawa, T. Kawahara and K. Yagi, Mater. Sci. Forum **389-393**, 319 (2002).
8. Lyle Patrick and W.J. Choyke, J. Phys. Chem. Solids **34**, 565 (1973).
9. T. Yamada and K.M. Itoh, Mater. Sci. Forum **389-393**, 675 (2002).
10. W.J. Choyke and Lyle Patrick, Phys. Rev. **B** 4, 1843 (1971).
11. L. Storasta, F.H.C. Carlsson, S.G. Sridhara, J.P. Bergman, A. Henry, T. Egilsson, A. Hallén and E. Janzén, Appl. Phys. Lett. **78**, 46 (2001).
12. A. Gali, P. Deák, E. Rauls, N.T. Son, I.G. Ivanov, E. Janzén and W.J. Choyke, submitted to Phys. Rev. **B** (2002).
13. W.J. Choyke, D.R. Hamilton and Lyle Patrick, Phys. Rev. **133**, A1163 (1964).
14. Lyle Patrick, W.J. Choyke, and D.R. Hamilton, Phys. Rev. **137**, A1515 (1965).
15. W.J. Choyke, D.R. Hamilton and Lyle Patrick, Phys. Rev. **139**, A1262 (1965).
16. Lyle Patrick, D.R. Hamilton, and W.J. Choyke, Phys. Rev. **143**, 526 (1966).
17. W.G. Spitzer, D.A. Kleinman and D. Walsh, Phys. Rev. **113**, 127 (1959).
18. W.G. Spitzer, D.A. Kleinman and C.J. Frosch, Phys. Rev. **113**, 133 (1959).
19. D.W. Feldman, J. H. Parker, Jr., W.J. Choyke and Lyle Patrick, Phys. Rev. **173**, 78 (1968).
20. B. Dörner, H. Schober, A. Wonhas, M. Schmitt and D. Strauch, Eur. Phys J. **B 5**, 839 (1998).
21. J. Serrano, J. Strempfer, M. Cardona, M. Schwoerer-Böhning, H. Requardt, M. Lorenzen, B. Stojetz, P. Pavone and W.J. Choyke, Appl. Phys. Lett. **80**, 4360 (2002).
22. J. Serrano, J. Strempfer, M. Cardona, M. Schwoerer-Böhning, H. Requardt, M. Lorenzen, B. Stojetz, P. Pavone and W.J. Choyke, Proc. ECSCRM 2002, to be published in Mater. Sci. Forum (2003).
23. W.J. Choyke, Inst. Phys. Conf. Ser. **142**, 257 (1996).
24. I.G. Ivanov, U. Lindefelt, A. Henry, O. Kordina, and C. Hallin, Phys. Rev. B **58**, 13634 (1998).
25. O. Shigiltchoff, T. Kimoto, D. Hobgood, P.G. Neudeck, L.M. Porter, R.P. Devaty and W.J. Choyke, Mater. Sci. Forum **389-393**, 921 (2002).
26. O. Shigiltchoff, S. Bai, R.P. Devaty, W.J. Choyke, T. Kimoto, D. Hobgood, P.G. Neudeck and L.M. Porter, Proc. ECSCRM2002, to be published in Mater. Sci. Forum (2003).
27. For example, see E.H. Rhoderick and R.H. Williams, *Metal-Semiconductor Contacts* (Oxford, Clarendon Press, 1988).
28. J.H. Werner and H.H. Güttler, J. Appl. Phys. **69**, 1522 (1991).
29. R.T. Tung, Phys. Rev. B **45**, 13509 (1992).
30. J. Osvald, J. Appl. Phys. **85**, 1935 (1999).
31. J. Osvald and E. Burian, Solid-State Electron. **42**, 191 (1998).
32. K. Maeda, Surf. Sci. **493**, 644 (2001).
33. R.H. Fowler, Phys. Rev. **38**, 45 (1931).
34. H.-J. Im, Y. Ding, J.P. Pelz and W.J. Choyke, Phys. Rev. B **64**, 075310 (2001).